Journal of Power Sources 196 (2011) 9299–9307

Contents lists available at ScienceDirect

Journal of Power Sources

journal homepage: www.elsevier.com/locate/jpowsour

Enhanced electrocatalytic activity of platinum supported on nitrogen modified ordered mesoporous carbon

YunXia Guo, JianPing He*, Tao Wang, HaiRong Xue, Yuanyuan Hu, Guoxian Li, Jing Tang, Xing Sun

College of Material Science and Technology, Nanjing University of Aeronautics and Astronautics, Nanjing, Jiangsu 210016, PR China

ARTICLE INFO

Article history:
Received 2 June 2011
Received in revised form 23 July 2011
Accepted 24 July 2011
Available online 29 July 2011

Keywords:
Fuel cell
Mesoporous
Nitrogen modified
Platinum nanoparticles
Electrocatalytic activity

ABSTRACT

Nitrogen-modified ordered mesoporous carbon is synthesized via the 900 °C carbonization of polyaniline-coated mesoporous carbon. The electronic states of nitrogen atoms are investigated by XPS technique. Pyridinic nitrogen and quaternary nitrogen generate disorders and curvatures on the surface of graphitic carbon layers with nitrogen atoms replacing carbon atoms at the edges and the interior of carbon stacking, and thus offering beneficial anchoring sites for $PtCl_6^{2-}$ ions. Pyridinic nitrogen and pyrrolic nitrogen offer p electrons to the sp^2 hybridized graphitic carbon layers, decreasing the inner electrical resistance of the catalytic carbon layer, enhancing the rate of proton diffusion, and transporting more free electrons to oxidative platinum. Due to the advantageous modification of the electronic structure of carbon atoms, platinum nanoparticles with a narrow size distribution are homogenously dispersed onto the surface of nitrogen-modified ordered mesoporous carbon, as evidenced by TEM images. Electrochemical tests show that the samples loaded platinum calcined at the 900 °C exhibit the optimum loading performance among as-made catalysts and a gradually decreased decay in electro-catalytic activity with time, with the current density stabilized at 3.64 mA cm^{-2}, which is far higher than that of mesoporous carbon (0.15 mA cm^{-2}).

1. Introduction

Polymer electrolyte membrane fuels cells (PEMFC) and direct methanol fuel cells (DMFC) has witnessed great developments over the last few decades [1]. Nevertheless, the commercial launch is still mainly hindered by the prohibitive production cost of noble metals, as well as relativity poor activity and durability [1–4]. Therefore, the successful preparation of desirable support materials is a prerequisite to obtain highly dispersed platinum or platinum-based alloy nanoparticles with a narrow size distribution. Recently, ordered mesoporous carbon (OMC) has been getting more and more attention due to its large specific surface area and mono-dispersed three-dimensionally interconnected mesopores, which are necessary to obtain highly and uniformly dispersed catalytic metal particles [5–9].

However, pristine OMC, as a support of catalysts, is generally prohibited by the poor supporting abilities occurred in facile microwave-assisted loading method, such as the non-ideal electrical conductivity, along with the poor surface chemistry and structure of support materials [10–12]. Consequently, the surface modification of OMC is much needed. The commonly utilized surface modification methods have been on the doping of heteroatoms to optimize the support materials, which is, after all, an effective route to prepare a catalyst with optimized structure and morphology. This doping strategy predicts a promising research prospective. Among various doping elements, the nitrogen atom has attracted more and more attention. Wu Gang's group has reported a novel shell-core structured N-doped spherical carbon [13]. Compared with non-modified carbon black, its electrochemical performance was enhanced. Xia's group has successfully fabricated polyaniline-(mesoporous) carbon composites via in situ polymerization of aniline applying self-made ordered mesoporous carbon (CMK-3) as carbon precursor, exhibiting excellent electrochemical capacitance [14]. Yung's group has made nitrogen-doped magnetic carbon utilizing as-synthesized polypyrrole as carbon source, showing relatively better electro-catalytic performance in comparison with Vulcan XC-72 supported Pt [15].

The present work was undertaken to intensively investigate the beneficial effect on the optimization of graphitic electrocatalytic layer, along with the corresponding mechanism interpretation. N-modified OMC was prepared via coating the surface of OMC with in situ polymerized polyaniline carbonized at different temperatures. Aniline, a low-cost and widely available raw material, can in situ polymerize into polyaniline. Since the aromatic carbon precursors can increase the graphitization degree in the preparation of mesoporous carbon [16]. The catalytic layer exhibits decreased electrical resistance, contributing to the proton diffusion and

* Corresponding author. Tel.: +86 25 52112900; fax: +86 25 52112626.
E-mail addresses: ynxia@nuaa.edu.cn (Y. Guo), jianph@nuaa.edu.cn (J.P. He), wangtao0729@nuaa.edu.cn (T. Wang), xuehairong123@163.com (H. Xue), huyuan8707@163.com (Y. Hu), lgx_nuaa@sina.com (G. Li), tang_jing@yahoo.cn (J. Tang), sunxing52199@163.com (X. Sun).

0378-7753/$ – see front matter © 2011 Elsevier B.V. All rights reserved.
doi:10.1016/j.jpowsour.2011.07.073

the reactant permeability into the electrocatalytic layer. Besides, various annealing temperatures were employed to determine the optimal electrical conductivity of N-modified OMC (C-N). Due to the existent imine groups, C-N-900 (C-N subjected to the 900 °C carbonization) displayed a relatively higher electrical conductivity than pristine OMC. Meanwhile, the highly integrated interconnected mesoporous structure was basically well preserved. Moreover, due to the disorders and curvatures derived from pyridinic N and quaternary N, the surface of graphitic carbon layers was much more advantageous to anchor $PtCl_6^{2-}$ ions. Therefore, such a carbon support showed remarkably enhanced electro-catalytic performance in sulfuric acid and methanol solution than pristine OMC. In addition, C-N-900/Pt presented a far higher current density stabilized at 3.64 mA cm^{-2} than that of OMC/Pt.

2. Experimental

2.1. Synthesis of catalysts

Ordered mesoporous carbon (OMC) was synthesized according to the method reported by Zhao's group [17]. C-N was prepared as follows: 0.1 g of as-made OMC powder was first dissolved into 30 ml of 0.1 M HCl under magnetically stirring, and subsequently 0.1 ml of aniline was in situ polymerized to prepare polyaniline using 0.25 g of ammonium persulfate (APS) and HCl as the initiator and the catalyst, respectively. Then the samples were repeatedly washed with de-ioned water and methanol, followed by the evaporation at 50 °C overnight, the resultant sample was denoted as C-N. Calcination treatment was carried out to carbonize C-N for 3 h under the N_2 flow rate of 20 L min^{-1} at varying temperatures consisting of 300 °C, 500 °C, 700 °C and 900 °C. The final samples were labeled as C-N-X, wherein, X denoted the carbonization temperature.

2.2. Preparation and electrochemical testing of catalysts

In a typical synthetic route, 1.4 mL of hexachloro-platinic acid (0.0386 M) was added into 20 mL of ethylene glycol solution by an ultrasonic stirring of 5 min to afford a yellowish solution, which was then adjusted to pH of slightly more than 9 with 2.5 M NaOH/ethylene glycol solution. Next, 40 mg of carbon powder was suspended into the above solution under 30 min of ultrasonic stirring. The obtained mixture was referred to the microwave-assisted heating. When cooling down to room temperature, the mixture was adjusted to the pH of 3 with 0.2 M HCl, and then centrifuged and washed with acetone and distilled water. The resulting centrifuged substance was vacuum dried for 12 h at 80 °C. The Pt loading weight percentage was theoretically 20 wt% [12].

2.3. Characterization

Structural properties of the carbon materials were measured by N_2 adsorption isotherm by using an ASAP 2010 Micrometitics at 77 K. X-ray diffraction (XRD, Bruker D8 ADVANCE) were recorded to characterize the ordered mesoporous structure and identity the crystallographic phases of catalysts. Transmission electron microscopy (TEM, 200 KV, FEI Tecnai G^2) was used as a routine technique to characterize the mesoscopic morphology. Thermogravimetry (TG) was to measure the variation in mass of a sample when it undergoes temperature scanning from room temperature to 900 °C under the N_2 flow rate of 10 L min^{-1}. X-ray photoelectron spectroscopy (XPS, ESCALAB 250, Thermo Electron Co., America), with K-Alpha emitted at the power of 150 W and the working voltage of 15 kV, is to yield the information on the elemental composition, the oxidation state of the elements and the quantitative analysis. Fourier transform infrared/Ramman spectroscopy (NEXU670) is performed to identify the generated functional groups. Inductively coupled plasma atomic emission spectrometry (ICP-AES, Jarrell-Ash 1100) is utilized to determine the total content percentage of one particular element in the composite. Four-probe electrical conductivity analyzer (Wentworth Laboratories 6514 System Electrometer Keithley) was to measure the electrical conductivity.

The cyclic voltammograms and chronoamperometry (CV, Solarton1287) were collected to evaluate the electrochemical properties using a three-electrode system. The working electrode was prepared as follows: suspend 5 mg of catalyst into the mixture of 1.0 mL of ethanol and 50 μL of Nafion (5 wt%) with 30 min of ultrasonic stirring; then, drop approximately 25 μL slurry onto the polished glassy carbon electrode to form a thin layer of ca. 0.1256 cm^2 in geometrical area. The platinum and the saturated calomel electrode were applied as the counter electrode and the reference electrode, respectively. Cyclic voltammetry was carried out in 0.5 M H_2SO_4 and 2.0 M CH_3OH + 1.0 M H_2SO_4 at a scan rate of 20 mV S^{-1}.

3. Result and discussion

3.1. Structural characterization of supports

As shown in Fig. 1a, small-angle XRD pattern of ordered mesoporous carbon (OMC) presented well-resolved (1 0 0), (1 1 0) and (2 0 0) diffraction peaks, indicating a 2D hexagonal mesoporous car-

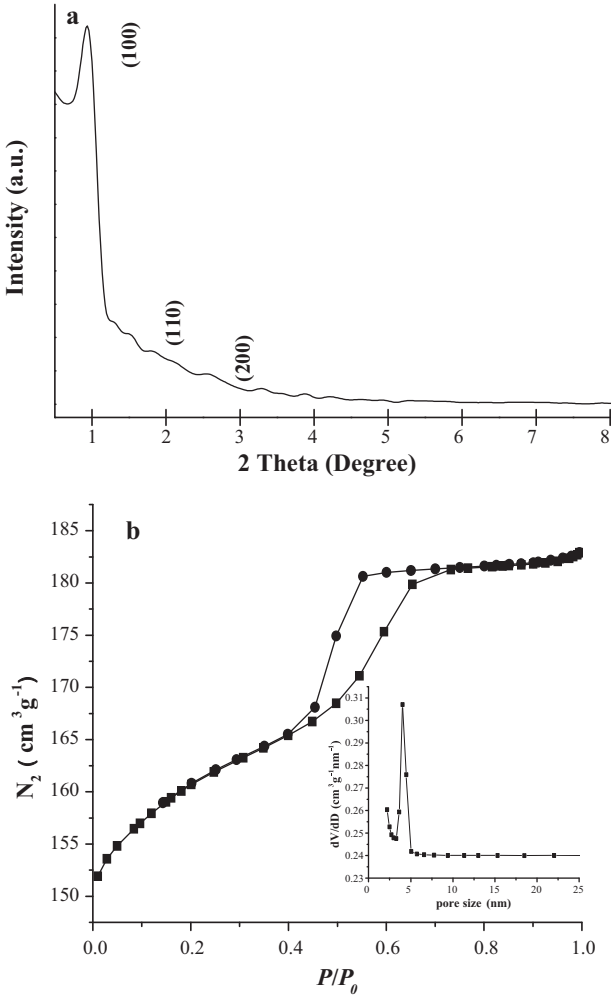

Fig. 1. Small-angle XRD pattern (a), and N_2 adsorption–desorption isotherm of ordered mesoporous carbon (OMC) with the inset of the pore size distribution calculated by the BJH model (b).

bon framework [18,5,19,20]. N_2 sorption isotherms and BJH pore size distribution (Fig. 1b) indicated a type-IV curve with a sharp capillary condensation step and an H1-type hysteresis loop, which is typical of large-pore mesoporous materials. OMC displayed a narrow size distribution centered at about 4 nm.

Fig. 2a showed the hexagonally packed strip-like arrays, suggestive of ordered mesoporous structure [21]. Fig. 2b presented the TEM image of C-N [22]. According to the synthesis process and the following Fourier transform infra-red spectra of OMC, it can be speculated that the flake-shaped transparent polyaniline was successfully coated onto the surface of OMC. C-N-900, achieved by 900 °C carbonization of C-N, was shown in Fig. 2c. Compared with the TEM image of OMC, C-N-900 was obviously lower in the definition of the 2-D hexagonal ordered mesoporous structure, indirectly indicating that C-N-900 had already coated by an N-doped layer. As the nitrogen and carbon atoms existent in C-N-900 were non-crystalline, the more precise electron diffraction characterization was non-available.

Fig. 3a showed FT-IR spectra of OMC, C-N, and polyaniline-modified OMC with different carbonization temperatures (C-N-X), wherein, X denoted the annealing temperature. The broad band at about 3400 cm^{-1} corresponds to –NH stretching vibration mode for N-containing samples (C-N and C-N-X), and –OH for OMC [23,24]. In Fig. 3b, the peaks located at 1590 cm^{-1} and 1494 cm^{-1} were assigned to the stretching vibration of C=N in –N=quinoid=N– and C=C in benzenoid ring, respectively [25–28]. The peak at 816 cm^{-1}, corresponding to the out-of-plane bending vibration, was assigned to the head-to-tail linkage among aniline monomers during in situ polymerization. The band of 1297 cm^{-1} was related to the C–H stretching vibration due to the aromatic conjugation, 1234 cm^{-1} associated with C=C in –N=quinoid=N– and 1170 cm^{-1} related to the in-plane bending vibration [28,29]. Besides, 598 cm^{-1} was signified as the resident Cl^{-1}, which was due to the added HCl as the catalyst of in situ polymerization reaction [30,31]. All these peaks detectable in C-N confirmed that polyaniline was successfully coated onto the surface of OMC. In Fig. 3a, with the calcination temperature increasing, the spectral line in the low wavenumber range became more and more smooth, indicating that the organic functional groups in OMC-polyaniline composite were gradually decomposed in a pyrolytic process. When C-N heated to 900 °C, mere imine group (C=N) was remnant, evidenced by the band of 1120 cm^{-1} [30,31]. Correspondingly, as to the samples carbonized at relatively lower temperatures, some hydrophobic organic groups still existed.

In Fig. 4, OMC showed a slight weight loss, as can be attributed to the evaporation of the water molecules absorbed from the air. And yet, much larger weight loss was observed for C-N sample. The thermal decomposition procedure for C-N sample can be divided into three steps. The first step, below 500 °C, presented 12.4% of weigh loss, which can be assigned to the HCl molecules detached from the backbone of polyaniline. Another 13% weight loss was detected for the following step with carbonization temperature up to 700 °C, attributed to the atoms loss originated from the broken benzene rings. The last step appeared much more weight loss up to 18.1%, mainly because most organic functionalities were decomposed into mere amine groups.

XPS, as a surface characterization technique, is commonly utilized to identify the surface elemental compositions and the chemical states. As can be seen from Fig. 5a, nitrogen atom was detected on the surface of C-N-900, showing that nitrogen atoms had doped into the surface of OMC. In C-N-900, carbon atoms were predominantly sp^2 hybridized denoted by the C_{1s} binding energy of 284.7 eV. The O_{1s} signal at 532.7 eV implied the presence of absorbed H_2O molecules [32]. The nitrogen atoms can incorporate into the carbon layers to replace the carbon atoms at different sites if subjected to the pyrolysis process with the temperature above

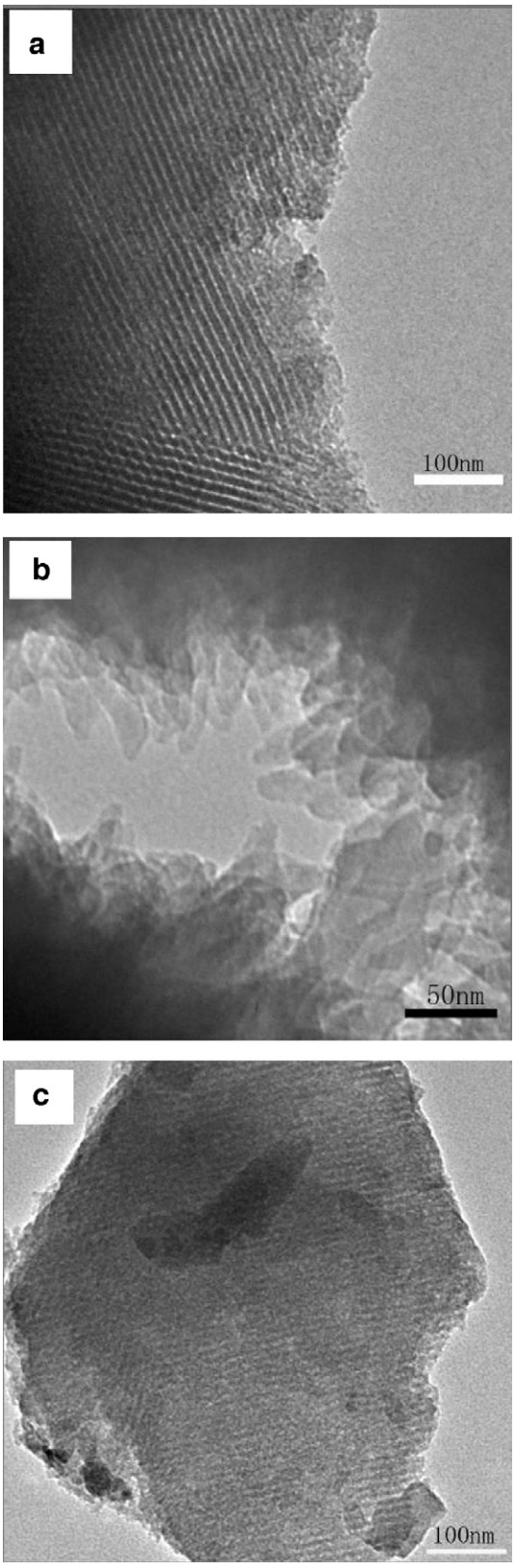

Fig. 2. TEM images of OMC (a), C-N (b) (without any carbonization) and C-N-900 (c).

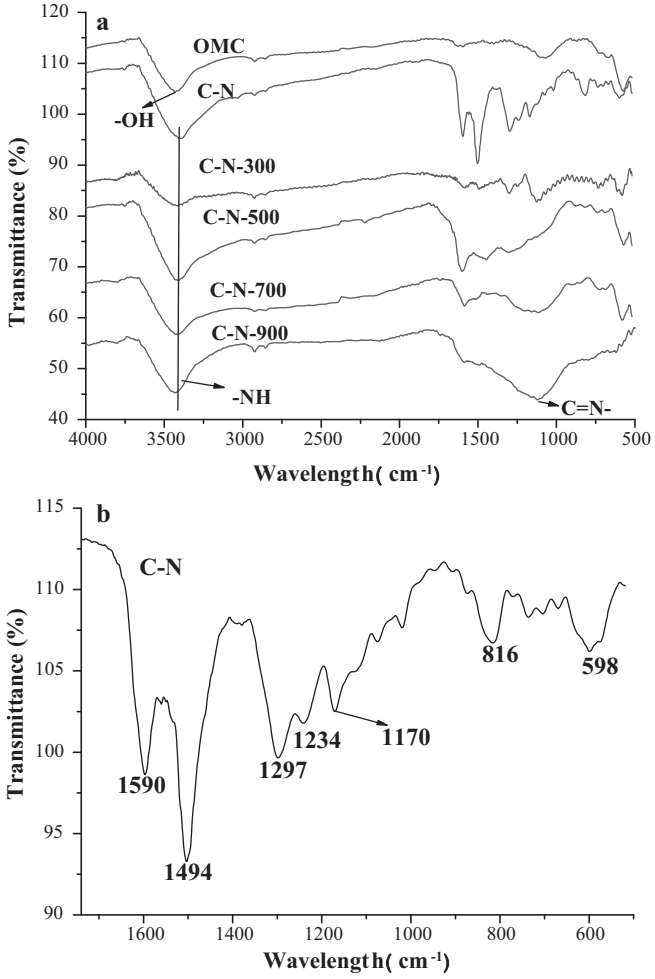

Fig. 3. Fourier transform infra-red spectra (FT-IR) of OMC and C-N-X (a) as well as C-N in a specific wavenumber range (b).

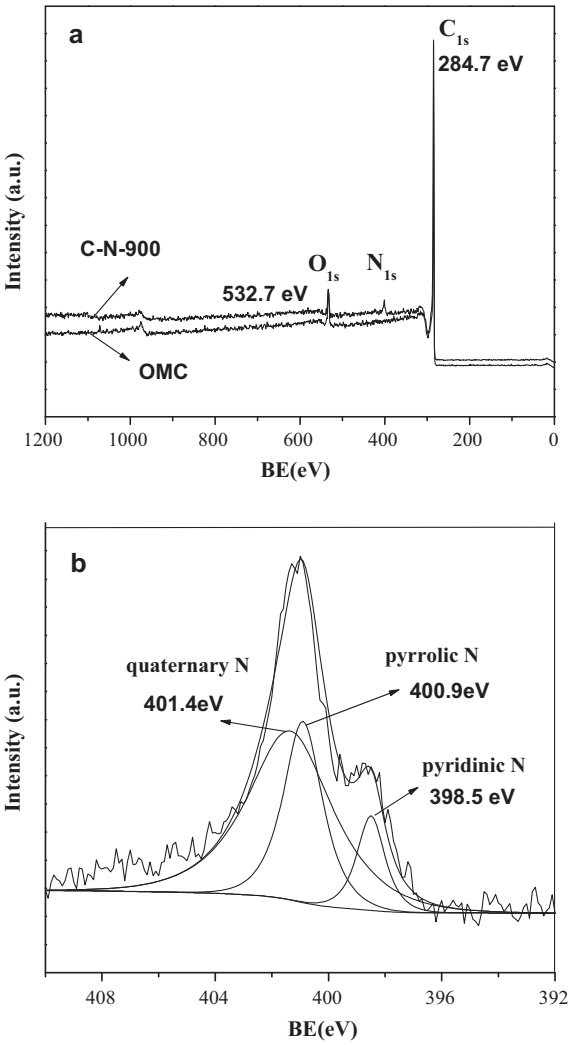

Fig. 5. XPS spectra of OMC and C-N-900 (a) together with C-N-900 N1s (b).

700 °C [13]. Therefore, N_{1s} exhibited various binding energies in the XPS spectra (Fig. 5b): pyridinic N (398.5 eV) referred to as N-6, pyrrolic N (400.8 eV) as N-5 and quaternary N (401.4 eV) as N-Q [33]. N-6 and N-Q atoms doped into the graphitic carbon structure to replace the carbon atoms at the edges of the graphitic carbon layers and inside the graphitic carbon planes, respectively [34]. N-5 atoms contributed one p electrons to the π system existent in N=C, while, N-6 atoms, assigned to N-C, provided two p electrons

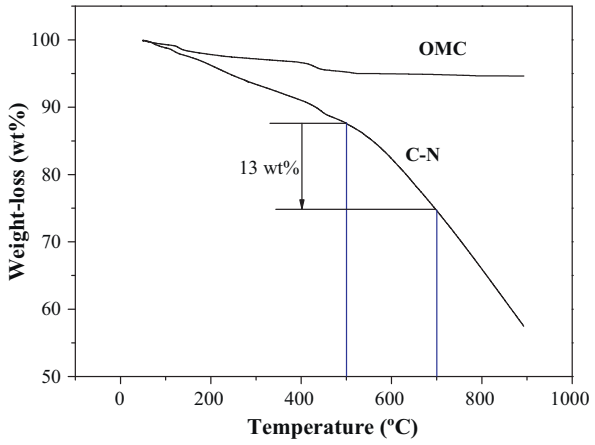

Fig. 4. TG curves for OMC and C-N sample.

[35–38]. Besides, due to the imine group detectable in FT-IR spectra, N-Q atoms was signified as =NH [38].

Table 1 listed the electrical conductivity of carbon materials. The electrical conductivity of C-N-700/900 was larger than that of OMC. Based on the previous analysis, the amine groups coated onto the surface of C-N-700/900 facilitated the increase of electrical conductivity, for the p electrons supplied by N-5 and N-6 atoms, along with the lone-pair electrons provided by N-Q atoms can enter into the sp^2 hybridized molecular orbits of graphitic carbon layers, and thus more free electrons can be transferred along the surface of the supports. However for C-N-300, the electrical conductivity was hardly detectable because of the slightly decreased electron delocalization and the weakened conjugation effect [39]. Such a phenomenon can be assigned to the following interpretation: the polymerized backbone chain of polyaniline fractured to a slight extent, and partial HCl molecules detracted from the quinoid amino group (–N=quinoid=N–) [40]. While for C-N-500, the backbone chain of polyaniline was thoroughly broken. Therefore, free electrons cannot be delocalized along the chain, and as a consequence, the electrical conductivity was negligible for C-N-300/500. Based on the above analysis, it can be inferred that, with the carbonization temperature going up, the electrical conductivity, mainly due to the increased graphitization degree, was prone to increase. However, a high carbonization temperature was extremely unfavorable for the well-preserved ordered mesoporous structure. In order to

Table 1
Electrical conductivity values of OMC and C-N-X.

Samples	OMC	C-N-300	C-N-500	C-N-700	C-N-900
Electrical conductivity ($S\,m^{-1}$)	2.24	Non-conductive	Approaching to 0	12.56	13.64

effectively preserve the perfect structure, a higher carbonization temperature above 900 °C was not referred to.

3.2. Characterization of Pt catalysts

Wide-angle XRD (Fig. 6), herein, was utilized to characterize the crystalline structure of the supported Pt catalyst. The broad diffraction at 2θ of about 23° corresponded to the carbon (0 0 2)-based plane diffraction. Four well-resolved diffraction peaks appeared at the Bragg angles of 39°, 46°, 67°, and 81° were indexed to (1 1 1), (2 0 0), (2 2 0), and (3 1 1) reflections of face-centered-cubic (fcc) structured Pt. Calculated by the formula of $D = 0.89\lambda/B\cos\beta$ based on the (2 2 0) reflection [41], the average Pt crystallite size is 3.1 nm for C-N-900/Pt and 4.2 nm for OMC/Pt.

Fig. 7 presented the TEM images and particle size distribution histograms of OMC/Pt and C-N-900/Pt catalysts, respectively. Pt nanoparticles in OMC/Pt presented a relatively random distribution, and large Pt aggregation clusters observed in several locations. However for C-N-900/Pt, Pt nanoparticles were homogenously distributed with a relatively narrow size distribution. It can be induced that the average Pt nanoparticle size supported onto the OMC and C-N-900 was about 4.2 and 3.1 nm, respectively, well consistent with the calculated XRD results. The high-resolution TEM of C-N-900/Pt was presented in Fig. 7c, specifying that Pt nanoparticles with a narrow size distribution were homogenously dispersed onto the carbon support. The deposition and reduction of metal particles, as demonstrated above, was largely dependent on the surface nanostructure of Pt catalysts. The coated electrocatalytic layer of C-N-900 favorably increased the electrical conductivity, which can reduce the inner electrical resistance of the catalytic layer and enhance the rate of proton diffusion [1–3]. Additionally, N-6 and N-Q atoms substituted carbon atoms at the edges and the interior of graphitic carbon layers to generate curvatures and disorders in the graphitic stacking, and thus producing more beneficial anchoring sites for $PtCl_6^{2-}$.

ICP methodology is to determine the content of Pt in OMC/Pt and C-N-X/Pt. According to the measured results, the content of Pt in C-N-300/Pt and C-N-500/Pt was basically negligible. While for C-N-700&900/Pt, the content of Pt was much higher, with C-N-900/Pt approaching the theoretical value of 0.189 $mg\,cm^{-2}$. Based on the analysis above, the surface structure of C-N-900 was modified in favor of depositing $PtCl_6^{2-}$ ions by the curvatures and disorders existent in the graphitic stacking, which were generated with nitrogen atoms substituting carbon atoms at the edges and the interior of graphitic carbon layers, and consequently, providing desirable deposition and reduction sites for $PtCl_6^{2-}$.

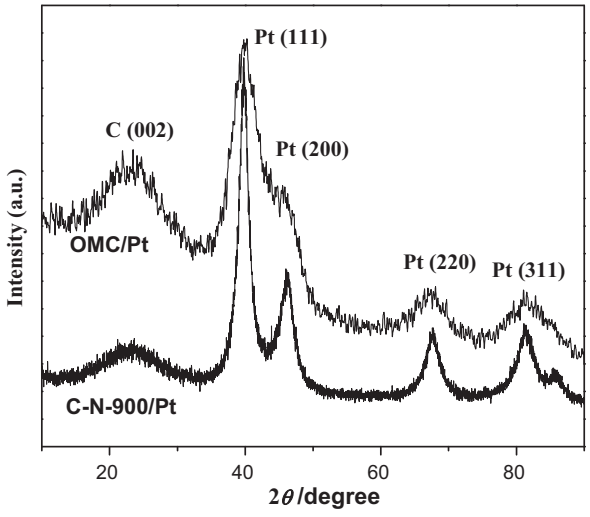

Fig. 6. Wide-angle XRD patterns of OMC/Pt and C-N-900/Pt.

Fig. 8 displayed Pt 4f region of the spectrum, which can be deconvoluted into two pairs of doublets. The relative quantitative analysis can be measured by the integrated intensities of the deconvoluted XPS signals and was shown in Table 2. Two peak doublets of 71.6/74.9 eV and 72.6/75.3 eV were observed in Fig. 8a, with the former indicative of metallic Pt and the later of Pt (II). Correspondingly, 71.3/74.6 eV and 72.7/75.2 eV were the signature of Pt (0) and Pt (II), respectively [42,43]. With the identical Pt loading, metallic Pt nanoparticles were more abundant on C-N-900/Pt than OMC/Pt. It should be noteworthy that the actual Pt loading for OMC/Pt was 2.4 wt%, and 19.5 wt% for C-N-900/Pt based on ICP analysis. The weight ratio of loaded metallic Pt between OMC/Pt and C-N-900/Pt was calculated to be 8.6:100. So C-N-900/Pt was much more favorable for the formation of metallic Pt, probably because more electrons on C-N-900/Pt derived from the doping of nitrogen atoms can be freely transferred along the planes of graphitic carbon layers, these electrons can be transferred to oxidative Pt, increasing the reduction probability of Pt ions.

3.3. Electrocatalytic performance

To compare the electro-catalytic properties [44,45] of supported Pt, CV curves are commonly referred to for electrocatalytic evaluation in Fig. 9, the corresponding electrochemical parameters were calculated and enumerated in Table 3. Wherein, EAS denoted an area where the electrolyte can reach in the porous structure of supports. As shown in Fig. 9a, The catalytic performance of C-N-900/Pt in H_2SO_4 and methanol was greatly improved, the interpretation for which can be summarized as follows: since nitrogen is more electronegative than carbon, it has been assumed that nitrogen groups change the electron donor/acceptor characteristics of carbon depending on their chemical states. For this reason, the coated electrocatalytic layer of C-N-900/Pt increased the electrical conductivity, and nitrogen supplied the sp^2 hybridized carbon atoms with much more electrons, which can be freely transferred along the planes of graphitic carbon stacking [46]. In such a way, the inner electrical resistance of the catalytic layer was reduced, and the rate of proton diffusion enhanced [1–3]. Besides, pyridinic N and quaternary N provided disorders and curvatures on the surface of graphitic carbon layers by virtue of nitrogen atoms replacing carbon atoms at the edges and the interior of carbon stacking, offering beneficial anchoring sites for $PtCl_6^{2-}$ ions. And the relatively more metal-

Table 2
Total content of Pt and valance states, binding energy (BE), and atomic ratios of integrated intensity (AR) of pure Pt in Pt/OMC and Pt/C-N-X.

Samples	Pt loading ($mg\,cm^{-2}$)	Pt (0)		Pt (II)	
		BE (eV)	AR (%)	BE (eV)	AR (%)
Pt/OMC	0.0228	71.6/74.9	50	72.6/75.3	50
Pt/C-N-700	0.164	–	–	–	–
Pt/C-N-900	0.185	71.3/74.6	71.8	72.7/75.2	28.2

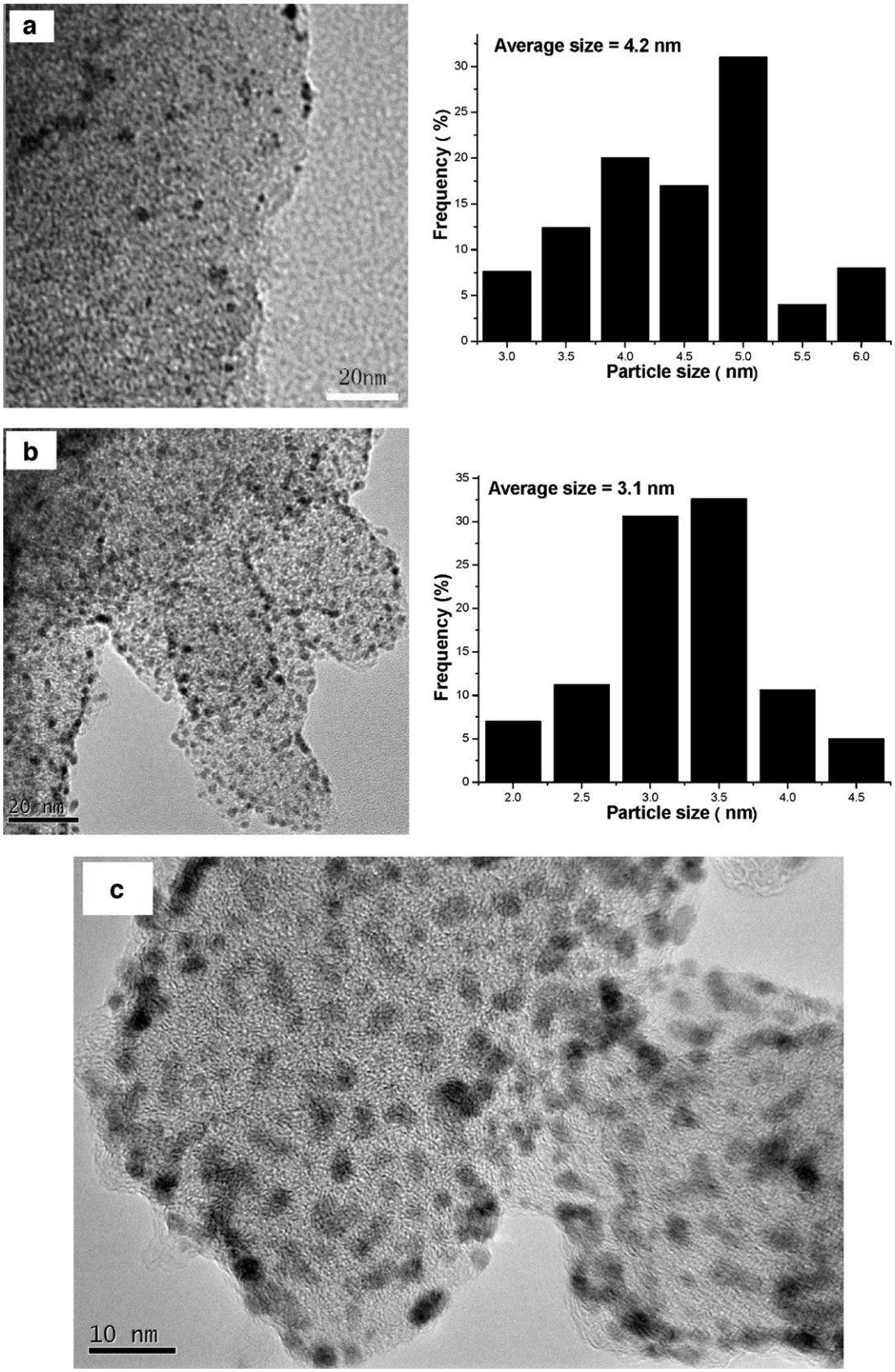

Fig. 7. TEM images and particle size distribution histograms of OMC/Pt (a) and C-N-900/Pt (b), and high-resolution TEM of C-N-900/Pt (c).

Table 3
Electro-catalytic parameters of Pt/C-E and Pt/C-N-X.

Samples	In H_2SO_4 (0.5 M)		In methanol			
	Q_H[a] (mC)	EAS[b] ($m^2\ g^{-1}$)	Onset voltage (V)	I_f[c] ($mA\ cm^{-2}$)	I_b[d] ($mA\ cm^{-2}$)	I_f/I_b
Pt/OMC	0.12	2.4	0.39	19.1	12.3	1.56
Pt/C-N-300	–	–	–	–	–	–
Pt/C-N-500	–	–	–	–	–	–
Pt/C-N-700	2.03	40.5	0.27	36.3	26.1	1.39
Pt/C-N-900	2.97	59.4	0.26	88.7	46	1.92

–: implies being hardly detectable.
[a] Total charge.
[b] Electrochemical active surface area.
[c] Forward scanning current density.
[d] Backward scanning current density.

lic Pt detected on the surface of C-N-900 can provide more active adsorption sites. This is also further evidenced by the electrochemical parameters in Table 3, wherein, the EAS of C-N-900 reached up to 59.4 $m^2\ g^{-1}$, significantly higher than that of OMC/Pt, because its high electrical conductivity facilitated enhancing the rate of proton diffusion, as can be also confirmed by the observed higher H_2 absorption and desorption peak currents. Herein, EAS was denoted as the H_2 reduction peak current (A) per unit mg of Pt in per unit area (cm^2).

Methanol electro-oxidation of all catalysts was shown in Fig. 9b. The onset potential was due to the breaking of C–H bonds and the removal of intermediates such as CO_{ad}, which can oxidize with OH_{ad} supplied by Pt-OH sites or other sources [47]. As shown in Fig. 10, at low potential, platinum atom can easily activate H_2O to supply the oxygen-containing species for the oxidative removal of CO species adsorbed on adjacent Pt active sites, thereby enhancing the tolerant ability for surface poison onto catalysts. For this reason, as shown in Table 3, the lowest onset potential of C-N-900 sample

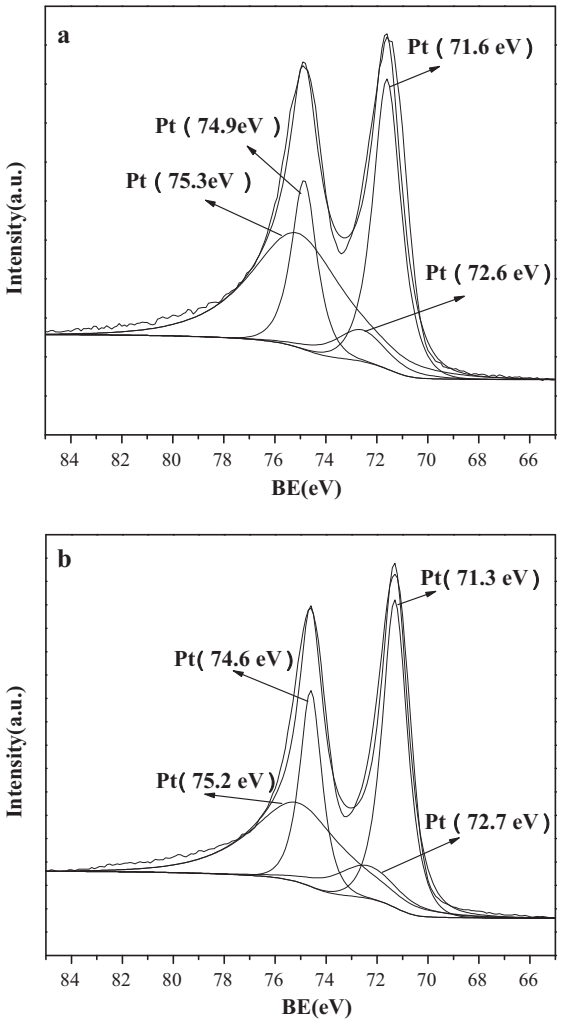

Fig. 8. XPS of OMC/Pt (a) and C-N-900/Pt (b).

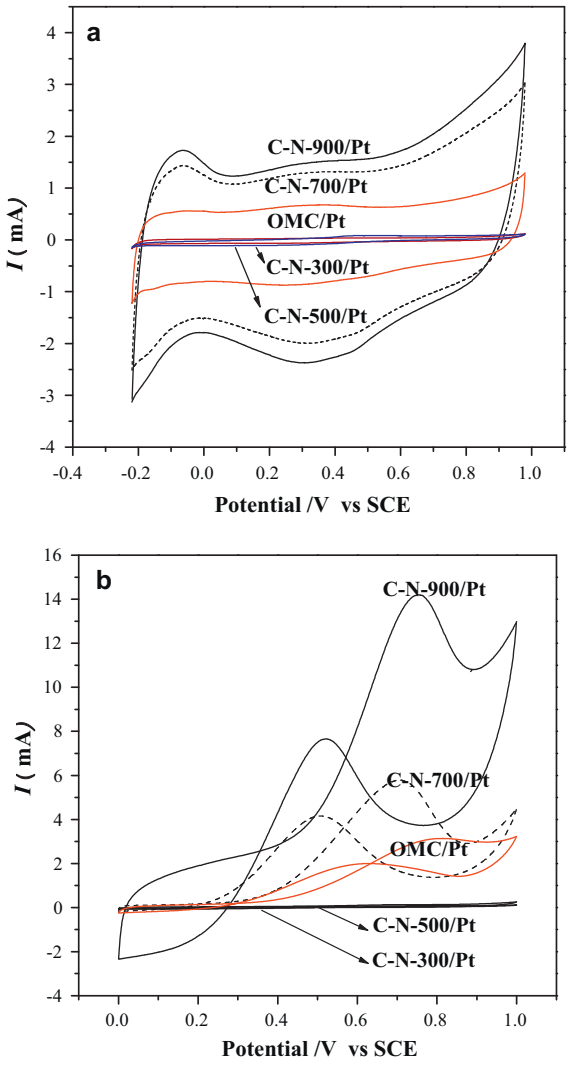

Fig. 9. CV curves of OMC/Pt together with C-N-X/Pt in H_2SO_4 (a) and methanol (b). Solid line: C-N-900/Pt, dotted line: C-N-700/Pt, red line: OMC/Pt. (For interpretation of the references to colour in this figure legend, the reader is referred to the web version of the article.)

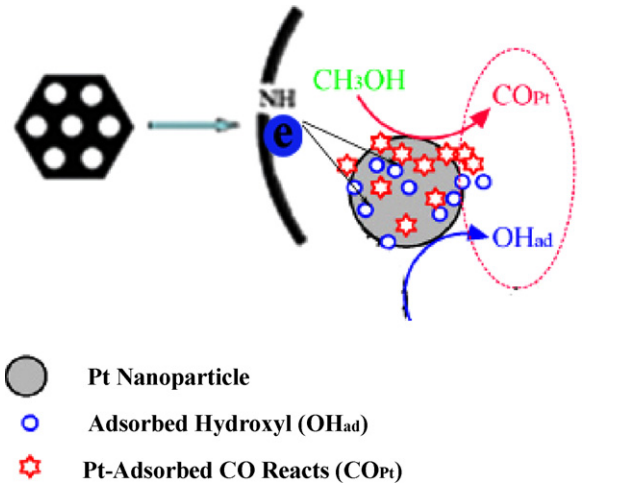

Fig. 10. Schematic illustration of a possible mechanism for electro catalysis of nitrogen modified OMC.

contributed to most favorable catalysis activity for methanol oxidation. Moreover, the ratio of the forward anodic peak current (I_f) to the reversed anodic peak current (I_b) was commonly used to determine the tolerance of catalysts to carbonaceous species accumulation [48]. A higher I_f/I_b value implied that methanol was more prone to be oxidized to CO. Furthermore, C-N-900/Pt possessed the highest oxidation peak current intensity in the forward and the backward scanning, an indication of a highest mass activity of Pt, mainly attributed to the highest utilization of Pt nanoparticles.

Chronoamperometric technique is an effective approach to evaluate the electrocatalytic activity and cyclic stability of catalysts. The current–time response was shown in Fig. 11 for methanol oxidation at a fixed potential of 0.52 V. C-N-900/Pt presented continuous decay in activity with time in the initial time range, but a gradually decreased decay in activity with time in the following time range. OMC/Pt showed a relatively stable decrease in activity with time in the whole time range. In the final stable region, C-N-900/Pt showed current density of 3.64 mA cm^{-2} however, OMC/Pt presented far lower current density of 0.15 mA cm^{-2}. Considering the far higher current density and a stable electrocatalytic activity reached in the last time range, the initial continuous decay for C-N-900/Pt in activity can be negligible.

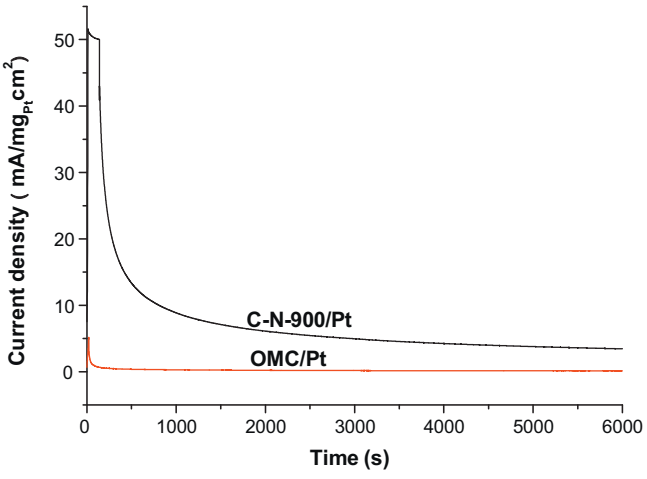

Fig. 11. Current–time curve at the potential of 0.52 V on C-N-900/Pt in 2.0 M CH_3OH + 1.0 M H_2SO_4 at a scan rate of 20 mV S^{-1}.

4. Conclusion

Amine group was introduced to modify ordered mesoporous carbon via the 900 °C carbonization of in situ polymerized aniline. More electronegativity of nitrogen than carbon contributed to change the electron donor/acceptor characteristics of carbon depending on their chemical states. In this case, pyridinic nitrogen and pyrrolic nitrogen offered more free p electrons to the sp^2 hybridized graphitic carbon layers, decreasing the inner electrical resistance of the catalytic carbon layer. Pyrrolic nitrogen and quaternary nitrogen generated disorders and curvatures on the surface of graphitic carbon layers with nitrogen atoms replacing carbon atoms at the edges and the interior of carbon stacking, offering beneficial anchoring sites for $PtCl_6^{2-}$ ions. Due to the favorable doping of nitrogen atoms, fine platinum nanoparticles were homogenously and densely dispersed on ordered mesoporous carbon, as further demonstrated by the enhanced electrocatalytic activity of the cyclic voltammograms in sulfuric acid and methanol. Therefore, nitrogen-doped ordered mesoporous carbon was more desirable as catalyst supports than pristine mesoporous carbon. This nitrogen-doped modification for carbon supports would be a promising technique in the future practical consideration.

Acknowledgements

The authors appreciate the financial support of the National Natural Science Foundation (50871053) and the Aeronautical Science Foundation of China (2007ZF52061).

References

[1] R. Borup, J. Meyers, B. Pivovar, S.Y. Kim, R. Mukundan, N. Garland, D. Myers, M. Wilson, F. Garzon, D. Wood, P. Zelenay, K. More, K. Stroh, Chem. Rev. 107 (2007) 3904–3951.
[2] Y.Y. Shao, G.P. Yin, Y.Z. Gao, J. Power Sources 171 (2007) 558–566.
[3] Y.Y. Shao, G.P. Yin, Z.B. Wang, Y.Z. Gao, J. Power Sources 167 (2007) 235–242.
[4] H.A. Gasteiger, S.S. Kocha, B. Sompalli, F.T. Wagner, Appl. Catal. B-Environ. 56 (2005) 9–35.
[5] F.B. Su, J.H. Zeng, X.Y. Bao, Y.S. Yu, J.Y. Lee, X.S. Zhao, Chem. Mater. 17 (2005) 3960–3967.
[6] W.C. Choi, S.I. Woo, M.K. Jeon, J.M. Sohn, M.R. Kim, H.J. Jeon, Adv. Mater. 17 (2005) 446–451.
[7] G.S. Chai, S.B. Yoon, J.S. Yu, J.H. Choi, Y.E. Sung, J. Phys. Chem. B 108 (2004) 7074–7079.
[8] H. Chang, S.H. Joo, C. Pak, J. Mater. Chem. 17 (2007) 3078–3088.
[9] J.S. Yu, S. Kang, S.B. Yoon, G. Chai, J. Am. Chem. Soc. 124 (2002) 9382–9383.
[10] K. Wikander, H. Ekstrom, A.E.C. Palmqvist, A. Lundblad, K. Holmberg, G. Lindbergh, Fuel Cells 6 (2006) 21–25.
[11] F. Su, X.S. Zhao, Y. Wang, J.Y. Lee, Micropor. Mesopor. Mater. 98 (2007) 323–329.
[12] J.H. Zhou, J.P. He, Y.J. Ji, Electrochim. Acta 52 (2007) 4691–4695.
[13] G. Wu, D. Li, C.S. Dai, D.L. Wang, L. Ning, Langmuir 24 (2008) 3566–3575.
[14] Y.G. Wang, H.Q. Li, Y.Y. Xia, Adv. Mater. 18 (2006) 2619–2623.
[15] B. Choi, H. Yoon, Y.E. Sung, Carbon 45 (2007) 2496–2501.
[16] Y. Shao, J. Liu, Y. Wang, Y.H. Lin, J. Mater. Chem. 19 (2009) 46–59.
[17] Y. Meng, D. Gu, F.Q. Zhang, Y.F. Shi, H.F. Yang, Z. Li, C.Z. Yu, B. Tu, D.Y. Zhao, Angew. Chem. Int. Ed. 44 (2005) 7053–7059.
[18] S.H. Joo, S.J. Choi, R. Ryoo, Nature 412 (2001) 169–172.
[19] Y. Meng, D. Gu, F.O. Zhang, Y.F. Shi, L. Cheng, D. Feng, Z.X. Wu, Z.X. Chen, Y. Wan, A. Stein, D.Y. Zhao, Chem. Mater. 18 (2006) 4447–4464.
[20] R.L. Liu, Y.F. Shi, Y. Wan, Y. Meng, F.Q. Zhang, D. Gu, Z.X. Chen, B. Tu, D.Y. Zhao, J. Am. Chem. Soc. 128 (2006) 11652–11662.
[21] Y. Meng, D. Gu, F.Q. Zhang, Y.F. Shi, H.F. Yang, Z. Li, C.Z. Yu, Angew. Chem. Int. Ed. 44 (2005) 7053–7059.
[22] Y.J. Gu, W.T. Wong, Langmuir 22 (2006) 11447–11452.
[23] C.A. Amarnath, S. Palaniappa, A. Puzari, P. Rannou, A. Pron, Mater. Lett. 61 (2007) 4204–4207.
[24] X.B. Yan, Z.J. Han, Y. Yang, B.K. Tay, J. Phys. Chem. C 111 (2007) 4125–4127.
[25] D.W. Hatchett, M. Josowicz, J. Janata, J. Phys. Chem. B 103 (1999) 10992–10998.
[26] F. Cataldo, P. Maltese, Eur. Polym. J. 38 (2002) 1791–1803.
[27] J. Laska, Synth. Met. 129 (2002) 229–233.
[28] J. Stejskal, I. Sapurina, M. Tchchova, J. Prokes, Chem. Mater. 14 (2002) 3602–3606.
[29] J.S. Tang, X.B. Jing, B.C. Wang, Synth. Met. 24 (1988) 231–238.
[30] M. Trchovq, J. Stejakal, J. Proks, Synth. Met. 101 (1999) 840–841.
[31] E. Segal, O. Aviel, M. Narkis, Polym. Eng. Sci. 40 (2004) 1915–1920.
[32] S. Maldonado, K.J. Stevenson, J. Phys. Chem. B 108 (2004) 11375–11383.

[33] J. Lahaye, G. Nanse, A. Bagreev, V. Strelko, Carbon 37 (1999) 585–590.
[34] X.R. Zeng, Polymer 39 (1998) 1187–1195.
[35] J.R. Pels, F. Kapteijn, J.A. Moulijn, Q. Zhu, K.M. Thomas, Carbon 33 (1995) 1641–1653.
[36] S. Bhattacharyya, C. Cardinaud, G. Turban, J. Appl. Phys. 83 (1998) 4491–4500.
[37] S. Bhattacharyya, J. Hong, G. Turban, J. Appl. Phys. 83 (1998) 3917–3919.
[38] A.P. Dementjev, A. Graaf, V.D. Sanden, K.I. Maslakov, Diamond Relat. Mater. 9 (2000) 1904–1907.
[39] A.G.M. Diamid, J.C. Chiang, M. Halpem, Mol. Cryst. Liq. Cryst. 121 (1985) 173–180.
[40] X.H. Wang, Y.H. Geng, L.X. Wang, Synth. Met. 69 (1995) 265–266.
[41] S.L. Gojković, T.R. Vidakovic, D.R. Durovic, Electrochim. Acta 48 (2003) 3607–3614.
[42] J. Knecht, G. Stark, Z. Frencius, Anal. Chem. 289 (1978) 206–212.
[43] S. HuÈfner, G.K. Wertheim, Phys. Rev. B 11 (1975) 678–684.
[44] A. Pozio, D.M. Francesco, A. Cemmi, J. Power Sources 105 (2002) 13–19.
[45] R.Z. Yang, X.P. Qiu, H.R. Zhang, Carbon 43 (2005) 11–16.
[46] N.D. Kim, W. Kim, J.B. Joo, S. Oh, P. Kim, Y. Kim, J. Yi, J. Power Sources 180 (2008) 671–675.
[47] G. Wu, R. Swaidan, G. Cui, J. Power Sources 172 (2007) 180–188.
[48] Y. Lin, X. Cui, C. Yen, C.M. Wai, J. Phys. Chem. B 109 (2005) 14410–14415.